Fuel 123 (2014) 285–292

Contents lists available at ScienceDirect

Fuel

journal homepage: www.elsevier.com/locate/fuel

# $CH_4$ dissociation on the perfect and defective MgO(001) supported $Ni_4$

Hongyan Liu [a,b,c], Botao Teng [a,d], Maohong Fan [a,*], Baojun Wang [c,*], Yulong Zhang [e], H. Gordon Harris [a]

[a] Department of Chemical and Petroleum Engineering, University of Wyoming, 1000 E University Avenue, Laramie, WY 82071, USA
[b] College of Chemistry and Environment Engineering, Shanxi Datong University, Datong, Shanxi 037009, China
[c] Key Laboratory of Coal Science and Technology of Ministry of Education and Shanxi Province, Taiyuan University of Technology, Taiyuan, Shanxi 030024, China
[d] College of Chemistry and Life Sciences, Zhejiang Normal University, Jinhua, Zhejiang 321004, China
[e] Western Research Institute, Laramie, WY 82070, USA

## HIGHLIGHTS

- DFT method is employed to investigate the interaction between Ni and MgO.
- Charge transfers from MgO to adspecies through Ni are studied.
- Strong Ni–MgO interaction can increase the dissociation activity of $CH_4$.
- Calculation confirms that strong Ni–MgO interaction can resist carbon deposition.
- New design approaches for high activity and free-carbon catalysts are proposed.

## GRAPHICAL ABSTRACT

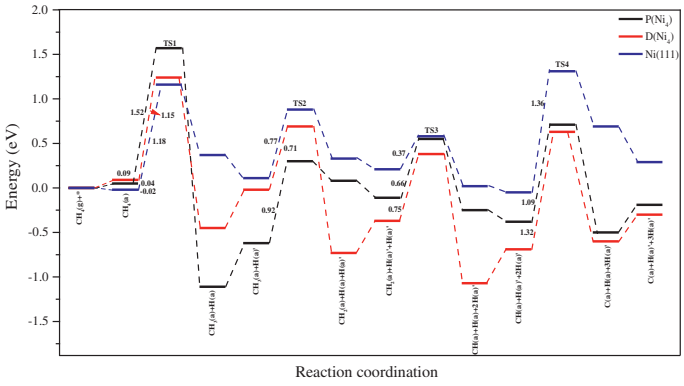


## ARTICLE INFO

*Article history:*
Received 18 October 2013
Received in revised form 24 December 2013
Accepted 25 January 2014
Available online 5 February 2014

*Keywords:*
$CH_4$ dissociation
Ni
MgO support
Metal-support interaction
Density functional theory

## ABSTRACT

A theoretical understanding of $CH_4$ dissociation on Ni-based catalysts is of great importance for the development of $CH_4$ reforming catalysts with high activity and carbon-deposition resistance. Based on comparisons of $CH_4$ dissociation on perfect and defective MgO supported $Ni_4$, as well as Ni(111), the effects of the strong interactions between $Ni_4$ and MgO on $CH_4$ dissociation are systematically investigated by density functional theory (DFT) calculations. Our results indicate that the interaction between $Ni_4$ and the defective MgO is stronger than for the perfect MgO. Consequently, the adsorptions of $CH_x$($x$ = 0–4) are weaker than those on the perfect $Ni_4$/MgO. Hirshfeld charge analysis shows that electrons are transferred from MgO to $Ni_4$, then to $CH_x$ adspecies; the stronger interactions between $Ni_4$ and MgO lead to less electronic transfer from $Ni_4$ to adspecies, which result in weaker adsorption of $CH_x$. Potential energy surface calculations of $CH_4$ dissociation indicate that there are lower energy barriers for the sequent dissociations of $CH_4 \rightarrow CH_2 + 2H$ and an appropriate barrier of CH oxidation matching up with that of $CH_2$ further dissociation on the model catalyst of $Ni_4$ supported on defective MgO. This might be an elementary requirement for an excellent $CH_4$ reforming catalyst, and may shed light on experimental catalyst development.


## 1. Introduction

The step dissociations of $CH_4$:

$$CH_4 \rightarrow CH_3 + H \quad (R1)$$

* Corresponding authors. Tel.: +1 307 766 5633; fax: +1 307 766 6777 (M. Fan). Tel.: +86 351 6018239; fax: +86 351 6041237 (B. Wang).
*E-mail addresses:* mfan@uwyo.edu (M. Fan), wangbaojun@tyut.edu.cn (B. Wang).

http://dx.doi.org/10.1016/j.fuel.2014.01.087
0016-2361/

$$CH_3 \rightarrow CH_2 + H \quad (R2)$$

$$CH_2 \rightarrow CH + H \quad (R3)$$

$$CH \rightarrow C + H \quad (R4)$$

are very important for $CH_4/CO_2$ reforming to produce syngas (CO and $H_2$) and reduce the emission of two major green-house gases, $CO_2$ [1–4] and $CH_4$. The key to $CH_4/CO_2$ reforming is to develop a catalyst with high reaction activity and good carbon deposition resistance [5–9]. Ni-based catalysts might have potential industrialization prospects, due to high activity and selectivity, as well as low cost. However, these catalysts must overcome a significant hurdle, i.e., carbon deposition, which leads to rapid deactivation. It has been found that oxide supports considerably affect the catalytic activity and carbon deposition on Ni-based catalysts in methane reforming with $CO_2$. Wei et al. [10] pointed out that Ni supported on nano-sized $ZrO_2$, MgO and $\gamma$-$Al_2O_3$ was highly active and stable. Hwang et al. [11] reported that clay-supported Ni exhibited high catalytic activities and long lifetimes. Similar results were obtained by Hou et al. [12] on $Al_2O_3$-supported Ni based catalysts.

Among all kinds of oxide supports, MgO is one of best choices for Ni-based catalysts owing to its large and relatively well-defined surface structure and stoichiometry [13], as well as its low oxygen vacancy formation energy. Experimental results suggest that defects on MgO have significant effects on the morphologies and properties of Ni-based catalysts [14–16]. Hu and Ruckenstein [17–21] found that a NiO/MgO catalyst had excellent anti-coking performance, which was attributed to the high dispersion of reduced Ni species, basicity of the support surface, and strong nickel-support interaction [22]. Feng et al. [23] reported that the NiO/MgO catalyst showed a higher activity after calcination at 800 °C, which was mainly due to the strong interactions between metal and support. Although the experimental results show that MgO might greatly improve the performance of Ni-based catalysts in $CH_4$ reforming, the electronic nature of the effect of the interaction between Ni and MgO on $CH_x$ adsorption, as well as the reaction mechanism and carbon deposition in the $CH_4/CO_2$ reforming process is still uncertain.

Rapid development of the density functional theory (DFT) technique has resulted in a powerful tool for understanding chemical reactions and designing catalysts at an atomic level [24–27]. DFT has been used to investigate the dissociation of $CH_4$ on pure Ni [28–30], Pt [31], Rh [32], as well as the strong interactions between metal and support on adsorption and reaction [33–36]. Studies on the interaction of metal Ni and support MgO have been reported [37,38], however, to the best of our knowledge, the effect of the interaction between Ni and MgO on $CH_x$ adsorption and dissociation of $CH_4$ on Ni/MgO catalyst, as well as their electronic nature, have been seldom reported.

In this work, using the DFT method, the adsorption behaviors of $CH_x$ ($x$ = 0–4) and H, as well as the potential energy surfaces of $CH_4$ dissociations on perfect and defective MgO-supported $Ni_4$ are systematically investigated. The effects of the strong interactions between $Ni_4$ and MgO on $CH_x$ adsorption and $CH_4$ dissociation are systematically studied, and their corresponding electronic nature are explained by Hirshfeld charge analysis.

## 2. Computation details

### 2.1. Computational methods

The DFT calculations are performed using the Cambridge Sequential Total Energy Package (CASTEP) [39,40] in Material Studio 6.0 of Accelry Inc. All the calculations are conducted with the generalized gradient approximation (GGA) and the Perdew–Burke–Ernzerhof (PBE) exchange correlation function [41]. Ionic cores are described by ultrasoft pseudopotential [42] and the Kohn–Sham one-electron states are expanded in a plane wave basis with a cutoff energy of 340 eV. An electronic temperature of 0.1 $k_BT$ is utilized during calculations with the final results extrapolated to 0 K. Brillouin zone integration is approximated by a sum over special $k$-points using the Monkhorst–Pack method [43], which is set as $2 \times 2 \times 1$. Geometries are optimized until the following converging criteria are met: energy, force, and maximum displacement are converged to $2.0 \times 10^{-5}$ eV/atom, 0.05 eV/Å, and $2 \times 10^{-3}$ Å, respectively. Spin polarization is considered in all calculations. Transition states (TS) are located by using complete linear synchronous transit (LST) or quadratic synchronous transit (QST) methods [44]. Firstly, LST maximization is performed by an energy minimization in the directions conjugated to reaction pathway. Then, the TS approximation is used to perform QST maximization. From that point, another conjugate gradient minimization is carried out. The cycle had been repeated until a stationary point is located. The convergence criterion for transition state calculations was set to root-mean-square force of 0.25 eV/Å per atom.

The adsorption energy, $E_{ads}(X)$, is calculated as follows

$$E_{ads}(X) = E(X - Ni_4/MgO) - E(X) - E(Ni_4/MgO) \quad (E1)$$

where $X$ represents adsorbed species, $E(X - Ni_4/MgO)$ is the total energy of the species adsorbed on $Ni_4$/MgO, $E(X)$ is the energy of free $X$ species, and $E(Ni_4/MgO)$ is the energy of $Ni_4$/MgO. Therefore, a negative value corresponds to an energetically favorable adsorption. The adsorption energy of adspecies on $Ni_4$/MgO can be divided into the deformation energy of adspecies ($E_{def}(X)$), and catalyst ($E_{def}(Ni_4/MgO)$), as well as the interaction energy between adspecies and catalyst ($E_{int}$). Correspondingly, $E_{ads}(X)$ of adspecies can be expressed as

$$E_{ads}(X) = E_{def}(X) + E_{def}(Ni_4/MgO) + E_{int} \quad (E2)$$

$$E_{def}(X) = E(X') - E(X) \quad (E3)$$

$$E_{def}(Ni_4/MgO) = E(Ni_4/MgO') - E(Ni_4/MgO) \quad (E4)$$

$$E_{int} = E(X\text{-}Ni_4/MgO) - E(X') - E(Ni_4/MgO') \quad (E5)$$

where $E(X')$ and $E(Ni_4/MgO')$ are the energies of the deformed configurations for the $X$ species and substrate after adsorption, respectively. Meanwhile, the energy of strong metal-support interaction (SMSI) is defined as:

$$E_{SMSI} = E(X\text{-}Ni_4/MgO) - E(X\text{-}Ni_4') - E(MgO') \quad (E6)$$

where $E(X\text{-}Ni_4')$ and $E(MgO')$ represent the energy of $Ni_4$ cluster and MgO substrate upon adsorption, respectively.

### 2.2. Models

A $Ni_4$/MgO(0 0 1) modeling catalyst, which has been proved to be very stable and representative of Ni-based catalysts in the literature, is used in the present work [45–47]. The lattice constant of MgO(001) is optimized to be 4.301 Å, which is consistent with the experimental value, 4.213 Å [48]. A four-layer MgO(001) slab is used for both perfect and defective $Ni_4$/MgO catalysts, in which the bottom two layers are fixed in bulk position [49]. The defective $Ni_4$/MgO modeling catalyst is established by removing a neutral oxygen atom from the surface of MgO(001) [50,51].

## 3. Results

### 3.1. MgO(001) supported $Ni_4$ cluster

#### 3.1.1. Perfect surface

The most stable adsorption configuration of $Ni_4$ cluster on the perfect MgO(001) surface is selected as the model catalyst, and denoted as P($Ni_4$). Its structure is shown in Fig. 1(a), and the corresponding geometrical parameters are listed in Table 1. In P($Ni_4$), three Ni atoms ($Ni_a$, $Ni_b$ and $Ni_c$) directly interact with three oxygen atoms of the support surface, while the $Ni_d$ atom is located at the bridge site between $Ni_a$ and $Ni_c$. It is noted that the $Ni_a$–$Ni_c$ bond in $Ni_4$ cluster is cleaved and elongated to 3.046 Å, which enhances the interaction between $Ni_4$ and MgO. Correspondingly, the $Ni_4$ cluster is deformed into a butterfly shape, and the dihedral angle $Ni_a$–$Ni_b$–$Ni_d$–$Ni_c$ of the tetrahedron is opened to 103.2°.

#### 3.1.2. Defective surface

To explore the effect of the defective MgO(001) surface on $CH_4$ dissociation, the structures of $Ni_4$ cluster on MgO(001) with an oxygen-vacancy were also investigated in the present work. The most stable configuration of $Ni_4$ on the defective MgO surface is denoted as D($Ni_4$) and shown in Fig. 1(b). This is different from the structure of $Ni_4$ on the perfect MgO(001); $Ni_b$ is located above the oxygen vacancy site and about 1.362 Å above the surface in D($Ni_4$). Meanwhile, similar sites of $Ni_a$, $Ni_c$ and $Ni_d$ are observed for D($Ni_4$). The dihedral angle $Ni_a$–$Ni_b$–$Ni_d$–$Ni_c$ of the tetrahedron expands to 119.4°, which is larger than that of P($Ni_4$).

The calculated interaction energies between $Ni_4$ and MgO are −3.72 eV for P($Ni_4$) and −5.06 eV for D($Ni_4$), respectively. Obviously, the stronger interaction occurs when $Ni_4$ is adsorbed on the defective MgO surface, in contrast with that of the perfect one. Compared with the values of $Ni_4$ on spinel-like and non-spinel $Al_2O_3$ (−2.27 and −2.79 eV) [52], $Ni_4$ is more stable on MgO than on $Al_2O_3$.

In order to shed insight on the electronic interactions between $Ni_4$ and MgO support, Hirshfeld charges of $Ni_4$ are calculated and listed in Table 2.

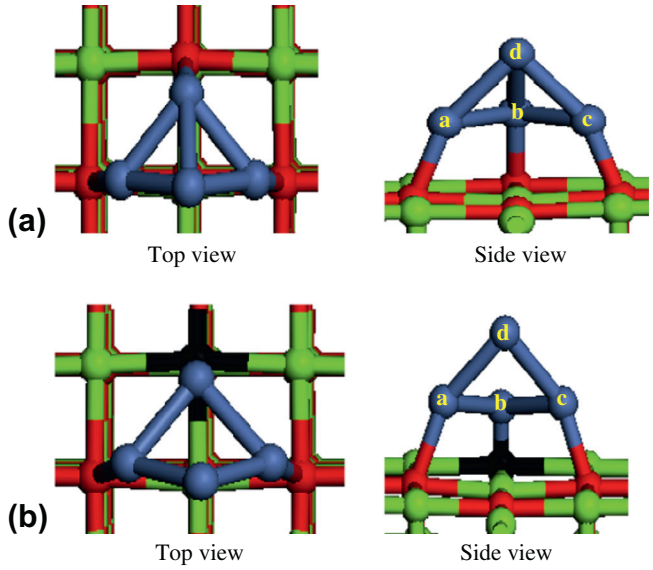


**Fig. 1.** Side and top views of $Ni_4$ supported on perfect and oxygen-vacancy MgO(001) surface (a) $Ni_4$ on the perfect MgO(001) surface and (b) $Ni_4$ on the defective MgO(001) surface (to visually show the location of the missing O atom, a black sphere was used to represent O vacancy).

As can be seen in Table 2, the total charges of $Ni_4$ in P($Ni_4$) and D($Ni_4$) are −0.22 and −0.37 e, respectively. The higher negative charge on $Ni_4$ in D($Ni_4$) indicates that more electrons are transferred from the defective MgO surface to $Ni_4$, which leads to the stronger interaction between MgO and $Ni_4$. This is consistent with the calculated interaction energy between $Ni_4$ and MgO. However, the charge transfer is different from the results by Li et al. [52], who observed that the electrons of $Ni_4$ cluster are transferred to γ-$Al_2O_3$ when $Ni_4$ cluster was deposited on γ-$Al_2O_3$. In addition, we further analyze the *d*-band structure of Ni(111) and $Ni_4$ supported on MgO, as shown in Fig. 2, and calculate the *d*-band center by E7 [53,54].

$$\varepsilon_d = \frac{\int_{-\infty}^{\infty} E\rho_d(E)dE}{\int_{-\infty}^{\infty} \rho_d(E)dE} \quad \text{(E7)}$$

where $\rho_d$ represents the density of states projected onto the Ni atoms' *d* band; *E* is the energy of *d*-band. As shown in Fig. 2, the *d*-band of $Ni_4$ in D($Ni_4$) becomes narrow compared to that in P($Ni_4$) and Ni(111). The calculated *d*-band centers of Ni(111), P($Ni_4$) and D($Ni_4$) are −1.42, −1.21 and −1.19 eV, respectively. Obviously, the *d*-band centers of P($Ni_4$) and D($Ni_4$) upshift to the Fermi level compared to that of Ni(111). In general, the closer the *d*-band center to the Fermi level, the more reactive is the catalyst [55]. Therefore, the possible activity order of the three model catalysts might be: D($Ni_4$) > P($Ni_4$) > Ni(111). However, this deduction should be further tested, according to the potential energy surface of the $CH_4$ dissociation reaction, due to the strong metal-support interaction between Ni and MgO.

### 3.2. $CH_4$ dissociation

To give a deeper insight into the $CH_4$ dissociation mechanism, as well as the support effects of MgO, the potential energy surfaces (PES) of methane dissociation reactions on the perfect and defective MgO supported on $Ni_4$, are systematically investigated. For further comparison, the PES of $CH_4$ dissociation on Ni(111) without MgO reported in our previous work [25], is also discussed herein.

- $CH_4 \rightarrow CH_3 + H$

*$CH_4$ adsorption*: As shown in Fig. 3, $CH_4$ only molecularly adsorbs at the top site of $Ni_d$ atom. The geometrical parameters of $CH_4$ adsorbed on $Ni_4$/MgO are listed in Supporting Materials. The bond lengths of C–H on P($Ni_4$) and D($Ni_4$) remain 1.096 Å, which are the same as the free $CH_4$ molecule, indicating the very weak interaction between $CH_4$ and $Ni_4$/MgO. The distances of C–$Ni_d$ are 3.463 and 2.901 Å, and the adsorption energies are 0.05 and 0.09 eV on P($Ni_4$) and D($Ni_4$), respectively. The positive adsorption energies are consistent with that for $CH_4$ adsorption on spinel $Al_2O_3$ supported $Ni_4$ (0.04 eV) [52]. Similarly, when $CH_4$ adsorbs on Ni(111), the bond length of C–H is 1.097 Å with an adsorption energy of −0.02 eV, indicating their weak interaction. Based on the bond lengths of C–H and the adsorption energies above, the interactions between $Ni_4$ and MgO have little effects on the adsorption behaviors of $CH_4$ on $Ni_4$/MgO.

*$CH_3$ adsorption*: The most stable configurations of $CH_3$ on both $Ni_4$/MgO models are adsorbed at the bridge site of $Ni_c$ and $Ni_d$, in which a C–H bond points to the vicinal $Ni_d$ atom and the other two are located at the side of the $Ni_c$–$Ni_d$. The C–$Ni_d$ and C–$Ni_c$ bond lengths are 2.095 and 1.956 Å on P($Ni_4$), while 2.150 and 1.930 Å on D($Ni_4$), respectively. The C–H bonds, paralleled to the $Ni_c$–$Ni_d$ bond, are elongated to 1.139 and 1.124 Å on P($Ni_4$) and D($Ni_4$), respectively. Meanwhile, the other two C–H bonds are almost elongated to 1.105 Å. The corresponding adsorption energies are −2.36 and −1.89 eV on P($Ni_4$) and D($Ni_4$), respectively, which

**Table 1**
Interaction distances and relevant dihedral angles of the optimized structures of $Ni_4$/MgO system (bond in Å, and angle in °).

| | $Ni_a$–$Ni_b$ | $Ni_b$–$Ni_c$ | $Ni_c$–$Ni_d$ | $Ni_a$–$Ni_d$ | $Ni_b$–$Ni_d$ | $\Phi$($Ni_a$–$Ni_b$–$Ni_d$–$Ni_c$) |
|---|---|---|---|---|---|---|
| P($Ni_4$) | 2.225 | 2.239 | 2.296 | 2.320 | 2.342 | 103.2 |
| D($Ni_4$) | 2.269 | 2.321 | 2.232 | 2.272 | 2.895 | 119.4 |

**Table 2**
Hirshfeld charges for $Ni_4$/MgO and $CH_x$ ($x$ = 0–3) adsorbed on supported $Ni_4$/MgO (in e).

| | | P($Ni_4$) | D($Ni_4$) |
|---|---|---|---|
| $Ni_4$/MgO | $Ni_4$ | −0.22 | −0.37 |
| $CH_3$ /$Ni_4$/MgO | $CH_3$ | −0.12 | −0.10 |
| | $Ni_4$ | −0.09 | −0.25 |
| $CH_2$/$Ni_4$/MgO | $CH_2$ | −0.14 | −0.12 |
| | $Ni_4$ | −0.03 | −0.22 |
| CH/$Ni_4$/MgO | CH | −0.15 | −0.14 |
| | $Ni_4$ | −0.08 | −0.24 |
| C/$Ni_4$/MgO | C | −0.20 | −0.19 |
| | $Ni_4$ | −0.04 | −0.22 |
| H/$Ni_4$/MgO | H | −0.10 | −0.06 |
| | $Ni_4$ | −0.13 | −0.31 |

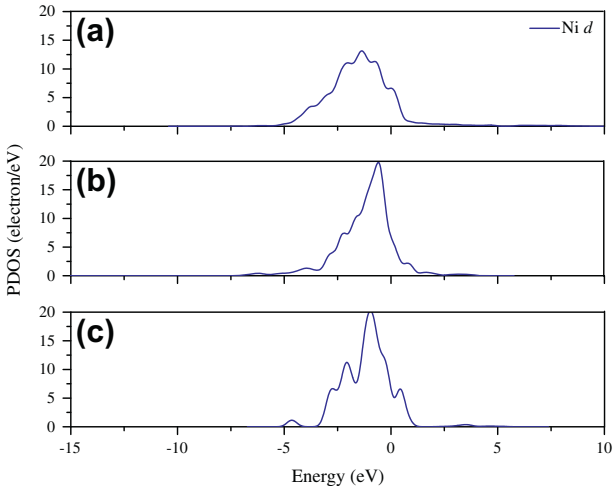


**Fig. 2.** The PDOS for $Ni_4$ on the three catalysts (a) Ni(1 1 1), (b) perfect $Ni_4$/MgO and (c) defective $Ni_4$/MgO.

are both stronger than that on Ni(1 1 1), −1.81 eV. Similar adsorption energy increase was also reported by Li et al. [52], in which $CH_3$ adsorbs at the interface (C bonded Al and Ni) with adsorption energy of −2.50 eV on $Ni_4/Al_2O_3$. These increases of adsorption energies on $Ni_4$/support might be attributed to the interaction of metal and support. To give insight into the support's effect on the adsorption of $CH_3$, the adsorption energies of $CH_3$ on both $Ni_4$/MgO are divided into three parts, as seen in Table 3. Obviously, the interaction energies between $CH_3$ and $Ni_4$ are the main contribution to the adsorption energies. The different interaction energies between $CH_3$ and $Ni_4$ are caused by the different interactions between supports and Ni. For further verification, Hirshfeld charge is analyzed. It can be seen from Table 2 that Hirshfeld charges of $CH_3$ are −0.12 and −0.10 e on P($Ni_4$) and D($Ni_4$); meanwhile the charges of $Ni_4$ are −0.09 and −0.25 e, respectively. Obviously, the sum of Hirshfeld charges of $CH_3$ and $Ni_4$ almost equals that of $Ni_4$ cluster on MgO before $CH_3$ adsorption. Therefore, from the electronic effect of the interaction between $Ni_4$ and MgO, it can be deduced that $Ni_4$ cluster firstly obtains electrons from the MgO support, and then transfers electrons to adspecies. Correspondingly, $Ni_4$ cluster on MgO acts as an electronic reservoir and conduit between the adspecies and support.

*H adsorption*: H prefers to adsorb at the bridge sites of $Ni_a$ and $Ni_d$ atoms of P($Ni_4$) and D($Ni_4$) surfaces to form two H–Ni bonds with bond lengths of 1.566–1.737 Å. The corresponding adsorption energies of H on P($Ni_4$) and D($Ni_4$) are −2.95 and −2.84 eV, respectively, which is slightly stronger than that on Ni(1 1 1)(−2.73 eV). Li et al. [52] reported that H prefers to adsorb at the interface between metal and support on the $Ni_4/\gamma$–$Al_2O_3$ with an adsorption energy of −2.96 eV, followed by another interface adsorption (−2.63 eV). We also examined the adsorption behaviors of H at the two similar sites on P($Ni_4$), and found that H only adsorbs on the interface between $Ni_4$ and perfect MgO with an adsorption energy of −2.73 eV, which is less stable than that at the bridge site of $Ni_a$ and $Ni_d$.

*$CH_4$ dissociates into co-adsorbed $CH_3$ and H*: When $CH_4$ adsorbed on the top of $Ni_d$ atom of P($Ni_4$) dissociates into $CH_3$ and H, one of the C–H bonds is elongated to 2.713 Å with C–$Ni_d$ and H–$Ni_d$ bond lengths of 1.935 and 1.530 Å, respectively, as seen in the transition state structure P(TS1); H then moves to the bridge site of $Ni_a$–$Ni_d$ with two H-Ni bonds of 1.601 and 1.617 Å. Meanwhile, the remaining $CH_3$ moves to the bridge site of $Ni_c$–$Ni_d$, and the C–$Ni_c$ and C–$Ni_d$ bonds are 1.980 and 2.032 Å, respectively. The activation energy barrier of $CH_4$ dissociation on P($Ni_4$) surface is 1.52 eV with an enthalpy change of −1.16 eV.

The dissociation of $CH_4$ on D($Ni_4$) is very similar to that on P($Ni_4$), with an energy barrier of 1.15 eV and enthalpy change of −0.54 eV. It was reported by Li et al. [52] that the $CH_4$ dissociation energy barrier is only 0.71 eV on $Ni_4/Al_2O_3$. Obviously, different supports ($Al_2O_3$ and MgO) result in different metal-support interactions, and further lead to different barriers in the $CH_4$ dissociation reaction.

- $CH_3 \rightarrow CH_2 + H$

*$CH_2$ adsorption*: $CH_2$ prefers to adsorb at the threefold site of $Ni_b$–$Ni_c$–$Ni_d$ on the perfect and defective MgO surfaces. The adsorption energies are −4.71 and −4.69 eV, respectively, which are both slightly stronger than that on Ni(1 1 1) (−4.66 eV). Similarly to the adsorption of $CH_3$ on $Ni_4$/MgO, the interaction between $CH_2$ and $Ni_4$ has the dominant contribution to $CH_2$ adsorption on $Ni_4$/MgO. Hirshfeld charges of $CH_2$ are −0.14 and −0.12 e on P($Ni_4$) and D($Ni_4$), respectively.

*$CH_3$ dissociates into co-adsorbed $CH_2$ and H*: For the dissociation of $CH_3$ on P($Ni_4$), the C–H bond is elongated to 2.652 Å in P(TS2), then H moves to the bridge site of $Ni_a$–$Ni_d$ and forms two H–Ni bonds with bond lengths of 1.577 and 1.682 Å. Meanwhile, the $CH_2$ fragment still remains at the bridge site of $Ni_c$ and $Ni_d$ atoms. The corresponding C–$Ni_c$ and C–$Ni_d$ are reduced to1.868 and 1.875 Å, respectively. The shorter C–Ni bond lengths in $CH_2$ on P($Ni_4$), compared with those in $CH_3$ on P($Ni_4$), indicate stronger interactions between $CH_2$ and P($Ni_4$) than those between $CH_3$ and substrate. The activation energy barrier of $CH_3$ dissociation on P($Ni_4$) is 0.92 eV, with an enthalpy change of −0.41 eV.

A similar structure was obtained for $CH_3$ dissociation on D($Ni_4$), as seen in D(TS2). The corresponding energy barrier and enthalpy change on D($Ni_4$) are 0.71 and −0.71 eV. Obviously, the activation energy on D($Ni_4$) is lower than that on the perfect $Ni_4$/MgO surface, and is the same as that on Ni(1 1 1).

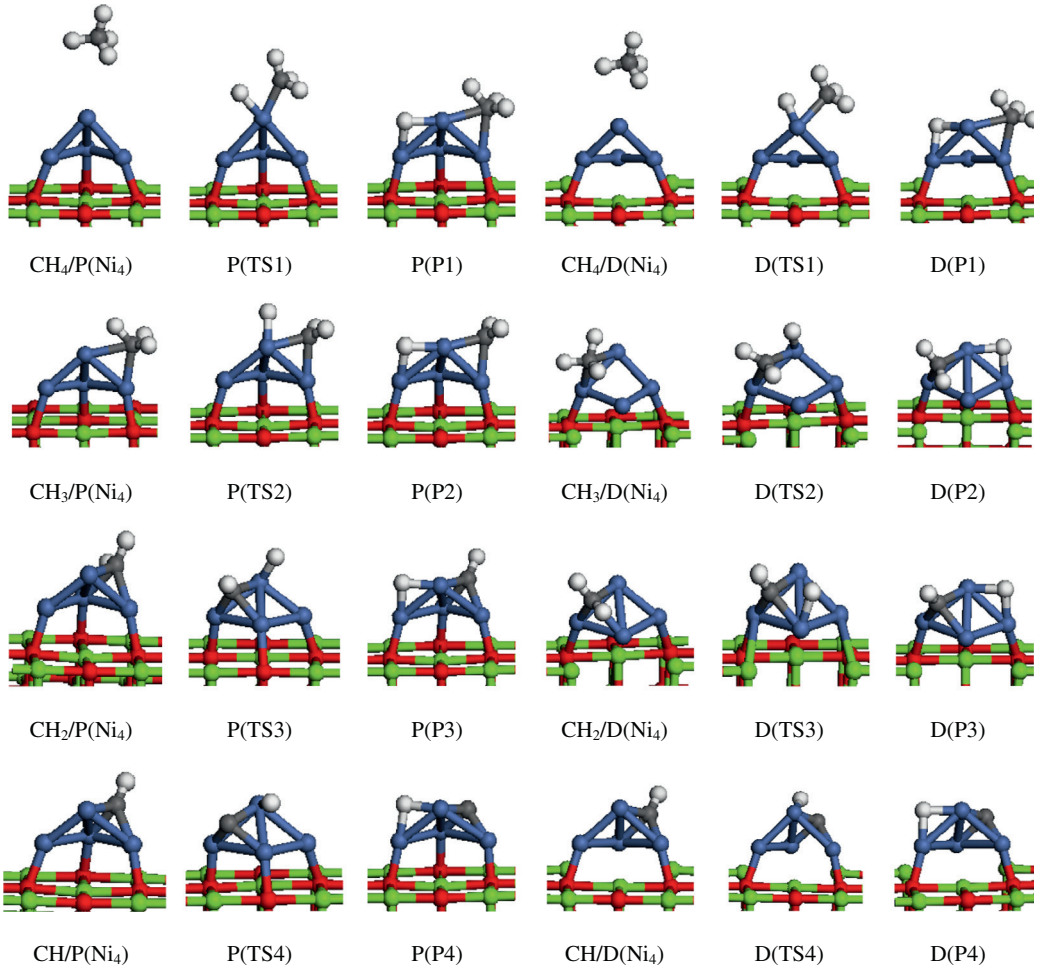


**Fig. 3.** Side view of the geometries of reactants, transition states, and products on the $Ni_4$/MgO (001) surfaces.

- $CH_2 \rightarrow CH + H$

*CH adsorption*: The most stable configurations of CH on P($Ni_4$) and D($Ni_4$) are shown in Fig. 3, in which the C atoms locate at the 3-fold site of $Ni_b$, $Ni_c$ and $Ni_d$ atoms. The C–Ni bond lengths are about 1.808–1.866 Å. The corresponding adsorption energies are −6.80 and −6.60 eV, respectively, which are also stronger than that on Ni(1 1 1), −6.24 eV. This can be attributed to the strong interaction between CH and $Ni_4$. Hirshfeld charges of CH are −0.15 and −0.14 e on P($Ni_4$) and D($Ni_4$), respectively.

*$CH_2$ dissociation into co-adsorbed CH and H*: Similar to the dissociations of $CH_4$ and $CH_3$, one of the C–H bonds is elongated to 2.385 Å for $CH_2$ dissociation, as seen in P(TS3). CH remains at the 3-fold site of $Ni_{b,c,d}$ atoms, while H moves to the bridge site of $Ni_a$–$Ni_d$ atoms. The activation barrier of $CH_2$ dissociation on P($Ni_4$) is 0.66 eV with an enthalpy change of −0.14 eV. Although the dissociation structure of $CH_2$ on D($Ni_4$) is very similar to that on P($Ni_4$), the corresponding energy barrier is 0.75 eV, which is relatively higher than that on P($Ni_4$). In addition, the dissociation barrier of $CH_2$ on Ni(1 1 1) is 0.37 eV, which is much lower than that on $Ni_4$/MgO surfaces. The enthalpy changes on D($Ni_4$) and Ni(1 1 1) are −0.70 and −0.19 eV, respectively.

- $CH \rightarrow C + H$

*C adsorption*: C prefers to adsorb at the threefold sites of Ni atoms on P($Ni_4$) and D($Ni_4$) surfaces, with adsorption energies of −7.73 and −7.52 eV, respectively, which is also stronger than that on Ni(1 1 1), −6.90 eV. As shown in Table 3, the increase of adsorption energies on $Ni_4$/MgO are mainly derived from the interaction energies of C and $Ni_4$. Furthermore, Hirshfeld charge of C is also the largest among $CH_x$ and H on the corresponding P($Ni_4$) and D($Ni_4$), which is consistent with its highest adsorption energy. Those results indicate that the more that electrons transfer to adspecies, the stronger adsorption of $CH_x$ on $Ni_4$/MgO.

*CH dissociates into co-adsorbed C and H*: The dissociation of the CH fragment on P($Ni_4$) is quite similar to that of $CH_2$, in which the C–H bond is elongated to 1.910 Å, and then is broken, as seen in P(TS4). The left C atom remains at the 3-fold site of Ni atoms; while the H atom moves to the bridge site of $Ni_a$–$Ni_d$. This dissociation reaction on P($Ni_4$) is exothermic with an enthalpy change of 0.12 eV, and the activation energy barrier is 1.09 eV. Similar dissociation process can be observed for CH via D(TS4) on D($Ni_4$) with an higher dissociation barrier of 1.32 eV and a lower enthalpy change of 0.09 eV. The dissociation energy barrier of CH on Ni(1 1 1) is 1.36 eV, with an enthalpy change of 0.55 eV.

## 4. Discussion

### 4.1. Potential energy surface of $CH_4$ dissociation

An ideal catalyst for $CH_4$ reforming should have a relatively high activity and selectivity and excellent resistance of

**Table 3**
Adsorption energy, deformation energy, and interaction energy for $CH_x$ ($x$ = 0–4) and H adsorption on $Ni_4$/MgO surfaces (in eV).

| | | P($Ni_4$) | D($Ni_4$) | Ni(1 1 1) |
|---|---|---|---|---|
| *$CH_4$* | | | | |
| | $E_{ads}$ | 0.05 | 0.09 | −0.02 |
| | $E_{def.substrate}$ | 0.03 | 0.02 | 0 |
| | $E_{def.X}$ | −0.02 | −0.02 | 0 |
| | $E_{int(X)}$ | 0.04 | 0.08 | −0.02 |
| | $E_{SMSI}$ | −3.03 | −5.04 | |
| *$CH_3$* | | | | |
| | $E_{ads}$ | −2.36 | −1.89 | −1.81 |
| | $E_{def.substrate}$ | 0.23 | 0.04 | 0.05 |
| | $E_{def.X}$ | 0.51 | 0.46 | 0.48 |
| | $E_{int(X)}$ | −3.10 | −2.39 | −2.34 |
| | $E_{SMSI}$ | −3.11 | −5.08 | |
| *$CH_2$* | | | | |
| | $E_{ads}$ | −4.71 | −4.69 | −4.66 |
| | $E_{def.substrate}$ | 0.38 | 0.17 | 0.04 |
| | $E_{def.X}$ | 0.45 | 0.45 | 0.01 |
| | $E_{int(X)}$ | −5.54 | −5.31 | −4.70 |
| | $E_{SMSI}$ | −3.46 | −5.26 | |
| *CH* | | | | |
| | $E_{ads}$ | −6.80 | −6.60 | −6.24 |
| | $E_{def.substrate}$ | 0.18 | 0.12 | 0.07 |
| | $E_{def.X}$ | 0.03 | 0.04 | 0.03 |
| | $E_{int(X)}$ | −7.01 | −6.76 | −6.22 |
| | $E_{SMSI}$ | −3.63 | −5.29 | |
| *C* | | | | |
| | $E_{ads}$ | −7.65 | −7.36 | −6.90 |
| | $E_{def.substrate}$ | 0.27 | 0.15 | 0.12 |
| | $E_{def.X}$ | 0.00 | −0.03 | 0 |
| | $E_{int(X)}$ | −7.92 | −7.48 | −6.92 |
| | $E_{SMSI}$ | −3.67 | −5.26 | |
| *H* | | | | |
| | $E_{ads}$ | −2.95 | −2.84 | −2.74 |
| | $E_{def.substrate}$ | 0.07 | 0.06 | −0.04 |
| | $E_{def.X}$ | 0 | 0 | 0 |
| | $E_{int(X)}$ | −2.85 | −2.89 | −2.70 |
| | $E_{SMSI}$ | −3.24 | −5.34 | |

carbon-deposition. The biggest difficulty for the catalyst development for $CH_4$ reforming is that a catalyst with high activity generally leads to a high rate of carbon-deposition. How to solve the dilemma? Could theoretical work shed light on this challenge? To explore the possible effects of MgO support on $CH_4$ dissociation and give an insight into the rate balance of catalytic activity and carbon deposition, the potential energy surfaces of the $CH_4$ dissociation on P($Ni_4$) (black line), D($Ni_4$)(red[1] line) and Ni(1 1 1) surface (blue line) are systematically calculated and shown in Fig. 4.

As shown in Fig. 4, $CH_x$(a) + H(a) denotes the co-adsorbed $CH_x$(a) and H(a); while $CH_x$(a) + H(a) + H(a)' denotes the co-adsorbed $CH_x$(a), H(a) and another isolated adsorbed H(a). It is well known that the first C–H bond dissociation is very difficult for its kinetically high energy barrier and thermodynamically endothermic reaction, as seen on the Ni(1 1 1) surface. However, it becomes a thermodynamically exothermic reaction for $CH_4 \rightarrow CH_3 + H$ dissociation when the $Ni_4$ cluster is supported on the perfect and defective MgO surfaces. Furthermore, the energy barrier of C–H dissociation on D($Ni_4$), 1.15 eV, slightly decreases compared with that on Ni(1 1 1), 1.18 eV, indicating a relatively high reaction rate of $CH_4$ dissociation when Ni nano-particles was supported on the defective MgO support.

For the dissociation of $CH_3$ intermediate, its energy barrier on D($Ni_4$) is also slightly lower than that on Ni(1 1 1). However, the energy barrier of $CH_2 \rightarrow CH + H$ reaction on D($Ni_4$) (0.75 eV) is much higher than that on Ni(1 1 1), 0.37 eV; meanwhile, the barriers of $CH \rightarrow C + H$ dissociation on D($Ni_4$) and Ni(1 1 1) are both as high as about 1.32–1.36 eV. It is well known that the dominant reason to deactivation for $CH_4$ reforming catalysts is carbon deposition, including the formation of fused ring carbon by the polymerization of CH fragments, as well as the graphite carbon by the aggregation of C atoms on the surface of catalysts. Both kinds of carbon deposition might cover the active site on Ni-based catalysts, leading to the rapid decrease in activity of $CH_4$ reforming. Due to the lower energy barrier of $CH_2$ dissociation on Ni(1 1 1), the rate of carbon deposition might be very high, which is consistent with the experimental facts that the initial activity of Ni nanoparticles is very high and decreases very fast when non-interaction exists between metal and support [56]. However, according to the comparison of energy barriers on Ni(1 1 1) and D($Ni_4$), the slightly lower energy barriers of the sequent dissociations of $CH_4 \rightarrow CH_2 + 2H$ and higher barriers of the $CH_2$ further dissociation on D($Ni_4$), indicate that the D($Ni_4$) catalyst has high activity of $CH_4$ reforming and good resistance of carbon deposition. This result is well consistent with the experimental data that the $CH_4$ dissociation rate is high and stable when Ni nano-particles was supported on MgO with high surface area, which might have more oxygen vacancies than the perfect one [57,58].

Different from $Ni_4$ cluster supported on the defective MgO support, the energy barrier of $CH_4 \rightarrow CH_3 + H$ reaction on P($Ni_4$) is much higher than those on Ni(1 1 1) and D($Ni_4$), which suggests a much lower activity of $CH_4$ reforming on P($Ni_4$). This calculation is also in good agreement with the experimental result, in which the catalysts of $Ni_4$ supported on MgO with the fine crystallization and low surface area have relatively low reaction rate of $CH_4$ reforming [57,58].

It was reported that $CH_x$ oxidation to $CH_xO$ [59–63] is also very important for $CH_4/CO_2$ reforming, which might reduce the corresponding carbon deposition. Therefore, the typical CH species oxidation behaviors on Ni(1 1 1), P($Ni_4$) and D($Ni_4$) are also involved in the present work. The corresponding geometries of reactions, intermediates and products are shown in Fig. 1S in Supporting Materials. On D($Ni_4$), the activation energy barrier of CH and O reaction is 0.64 eV, which is slightly lower than that on Ni(1 1 1)(0.80 eV) and much less than the value (1.17 eV) on P($Ni_4$) [28]. This result indicates that CH species on D($Ni_4$) is more prone to be oxidized to CHO and reduce the possible carbon deposition than on the perfect MgO support, which further support that Ni cluster on the defected MgO might be a good catalyst for $CH_4/CO_2$ reforming than on the perfect one.

Therefore, an excellent catalyst for $CH_4$ reforming should have the lower energy barriers of the sequent dissociations of $CH_4 \rightarrow CH_2 + 2H$, which means a high rate of $CH_4$ dissociation; furthermore, its barrier of the $CH_2$ further dissociation should match up with that of CH oxidation, which ensures that the CH species will be consumed instead of polymerizing to form the fused ring carbon deposition. This theoretical deduction points out the direction of the experimental efforts for the catalyst development of $CH_4$ reforming. Ni nano-particles supported on the defective MgO might be one of the good choices.

### 4.2. Effects of metal-support interactions on $CH_4$ reforming

According to the foregoing analysis, the adsorption energies of $CH_3$, $CH_2$, CH and C on D($Ni_4$) are generally relatively weaker than the corresponding ones on P($Ni_4$), which might be attributed to the

[1] For interpretation of color in Fig. 4, the reader is referred to the web version of this article.

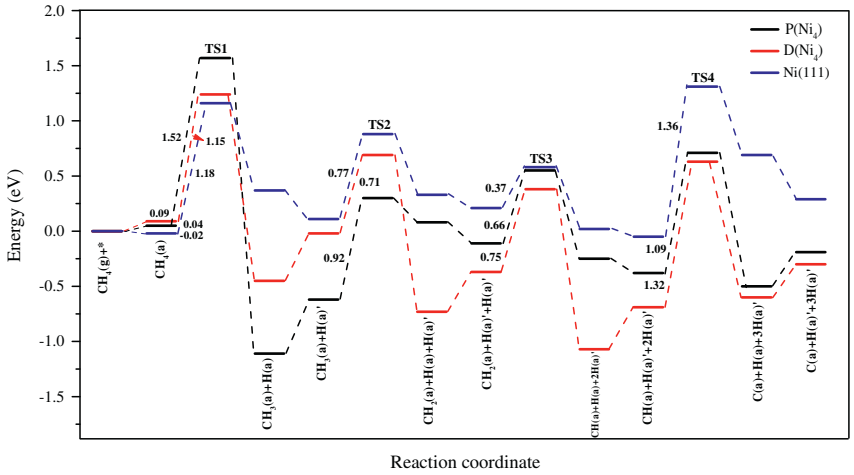


**Fig. 4.** Potential energy surfaces for $CH_4$ dissociation on the three catalysts (a) Ni(1 1 1), (b) perfect $Ni_4$/MgO and (c) defective $Ni_4$/MgO.

strong interactions between $Ni_4$ and MgO. As listed in Table 3, the interaction energies between $Ni_4$ and the perfect MgO vary from −3.03 to −3.67 eV; which are much less than those between $Ni_4$ and the defective MgO surface, −5.04 ∼ −5.34 eV. It seems that the stronger the interaction between metal and support, the weaker is the adsorption for $CH_x$ on $Ni_4$/MgO model catalysts. What is the electronic nature for this result? As seen in Table 2, the absolute charge values of $Ni_4$ on D($Ni_4$) are higher than those on P($Ni_4$), indicating that more electrons are transferred from support to $Ni_4$ clusters due to the stronger interaction between $Ni_4$ and the defective MgO surface. However, a few electrons are fed to the $CH_x$ adspecies, leading to the relatively weak adsorption energies.

On the other hand, the strong interaction between $Ni_4$ and the defective MgO also leads to the decrease in energy barriers of the sequent dissociations of $CH_4 \rightarrow CH_2 + 2H$ and an appropriate barrier of CH oxidation (0.64 eV) which matches up with that of $CH_2$ further dissociation (0.75 eV). This provides a way to develop new catalysts with high activity and good resistance of carbon deposition, that is, reducing MgO support to produce more oxygen vacancies, or dispersing Ni nano-particles on MgO with high surface area and more possible defects. This deduction is supported by the experimental facts that the reduced Ni/MgO catalysts have a higher activity and more excellent anticoking performance than those that are unreduced [19–22]. Another novel technique is to provide electronic donors by using additive reagents into the Ni/MgO catalysts to increase the interactions between Ni nano-particles and MgO. For example, Su et al. [64] reported that the $ZrO_2$ promoted Ni/MgO catalysts increase the electronic density of Ni, and further have relatively high activity and resistance of carbon deposition.

The calculated potential energy surfaces on D($Ni_4$) and P($Ni_4$) can be used to analyze the $CH_4$ dissociation from the perspectives of the reaction activation energies associated with the elementary reaction step. They are useful for design or development of cost-effective catalysts with desired activity and strong carbon-deposition resistance. According to the PES and the stronger interactions between Ni cluster and the defective MgO support than on P($Ni_4$) lead to the lower energy barriers of $CH_4 \rightarrow CH_2$ and more appropriate barrier for CH oxidation (0.64 eV), which is close to the $CH_2$ dissociation energy level (0.75 eV). The finding could lead a way for engineering the MgO supports with more oxygen vacancies and higher surface areas.

## 5. Conclusion

In the present work, the effects of the strong interactions between $Ni_4$ and MgO on the adsorptions of $CH_x$ and H as well as the sequent dissociations of $CH_4$ on perfect and defective MgO supported $Ni_4$ are systematically investigated by DFT calculation. It is demonstrated that $CH_4$ weakly adsorbs on $Ni_4$/MgO catalysts, while strong chemical adsorption occurs for $CH_3$, $CH_2$, CH, C and H atom. The interaction between $Ni_4$ and the defective MgO is stronger than with the perfect one, and the corresponding adsorption energies of $CH_x$($x$ = 0–3) and H are weaker than those on the perfect $Ni_4$/MgO. On the basis of Hirshfeld charge analysis, it is found that the stronger interactions between $Ni_4$ and MgO support lead to lower electronic feed from $Ni_4$ to $CH_x$ adspecies, resulting in weaker adsorption. Compared with $CH_4$ reaction on Ni(1 1 1) and P($Ni_4$), the energy barriers of the sequent dissociations of $CH_4 \rightarrow -CH_2 + 2H$ on D($Ni_4$) are relatively lower, while the barrier of CH oxidation matches up with that of $CH_2$ dissociation, which might lead to high activity and low carbon deposition rate. The present theoretical work should shed light on catalyst development for high performance $CH_4$ reforming.

## Acknowledgements

The work was supported by Wyoming Clean Coal Technology Fund in the U.S. and the National Natural Science Foundation of China (No. 21276171).

## Appendix A. Supplementary material

Supplementary data associated with this article can be found, in the online version, at http://dx.doi.org/10.1016/j.fuel.2014.01.087.

## References

[1] He L, Fan M, Dutcher B, Cui S, Shen X, Kong Y, et al. Dynamic separation of ultradilute $CO_2$ with a nanoporous amine-based sorbent. Chem Eng J 2012;189–190:13–23.
[2] Cui S, Cheng W, Shen X, Fan M, Russell AG, Wu Z, et al. Mesorporous amine-modified $SiO_2$ aerogel: A potential $CO_2$ sorbent. Energ Environ Sci 2011;4:2070–4.
[3] Dutcher B, Fan M, Leonard BM, Dyar DM, Tang J, Speicher EA, et al. Use of nanoporous FeOOH as a catalytic support for $NaHCO_3$ decomposition aimed at reduction of energy requirement of $Na_2CO_3$/$NaHCO_3$ Based $CO_2$ separation technology. J Phys Chem C 2011;115:15532–44.
[4] Zhang B, Fan M, Bland A. $CO_2$ separation by a new solid K-Fe sorbent. Energ Fuel 2011;25:1919–25.
[5] Efstathiou AM, Kladi A, Tsipouriari VA, Verykios XE. Reforming of methane with carbon dioxide to synthesis gas over supported rhodium catalysts: II. A steady-state tracing analysis: mechanistic aspects of the carbon and oxygen reaction pathways to from CO. J Catal 1996;158:64–75.
[6] Mark MF, Maier WF. $CO_2$-reforming of methane on supported Rh and Ir catalysts. J Catal 1996;164:122–30.
[7] Erdohelyi A, Cserenyi J, Solymosi F. Activation of $CH_4$ and its reaction with $CO_2$ over supported Rh catalysts. J Catal 1993;141:287–99.

[8] Liu H, Wang B, Fan M, Henson N, Zhang Y, Towler BF, et al. Study on carbon deposition associated with catalytic $CH_4$ reforming by using density functional theory. Fuel 2013;113:712–8.
[9] Bradford MCJ, Vannice MA. $CO_2$ reforming of $CH_4$ over supported Pt catalyst. J Catal 1998;173:157–71.
[10] Wei JM, Xu BQ, Li JL, Cheng ZX, Zhu QM. Highly active and stable Ni/$ZrO_2$ catalyst for syngas production by $CO_2$ reforming of methane. Appl Catal A 2000;196:L167–72.
[11] Hwang KS, Zhu HY, Lu GQ. New nickel catalysts supported on highly porous alumina intercalated laponite for methane reforming with $CO_2$. Catal Today 2001;68:183–90.
[12] Hou Z, Yokota O, Tanaka T, Yashima T. Investigation of $CH_4$ reforming with $CO_2$ on meso-porous $Al_2O_3$-supported Ni catalyst. Catal Lett 2003;89:121–7.
[13] Yang ZX, Wu RQ, Zhang QM, Goodman DW. Adsorption of Au on an O-deficient MgO(001) surface. Phys Rev B 2002;65:155407/1–7/8.
[14] Vitto AD, Pacchioni G, Delbecq F, Sautet P. Au atoms and dimers on the MgO(100) surface: a DFT of nucleation at defects. J Phys Chem B 2005;109:8040–8.
[15] Abbet S, Sanchez A, Heiz U, Schneider WD, Ferrari AM, Pacchioni G, et al. Acetylene cyclotrimerization on supported size-selected Pdn clusters ($1 \leqslant n \leqslant 30$): One atom is enough! J Am Chem Soc 2000;122:3453–7.
[16] Sanchez A, Abbet S, Heiz U, Schneider WD, Hakkinen H, Barnett RN, et al. When gold is not noble: nanoscale gold catalysts. J Phys Chem A 1999;103:9573–8.
[17] Hu YH, Ruckenstein E. Binary MgO-based solid solution catalysts for methane conversion to syngas. Catal Rev 2002;44:423–53.
[18] Hu YH, Ruckenstein E. The characterization of a highly effective NiO/MgO solid solution catalyst in the $CO_2$ reforming of $CH_4$. Catal Lett 1997;43:71–7.
[19] Hu YH, Ruckenstein E. An optimum NiO content in the $CO_2$ reforming of $CH_4$ with NiO/MgO solid solution catalysts. Catal Lett 1996;36:145–9.
[20] Ruckenstein E, Hu YH. The effect of precursor and preparation conditions of MgO on the $CO_2$ reforming of $CH_4$ over NiO/MgO catalysts. Appl Catal A 1997;154:185–205.
[21] Ruckenstein E, Hu YH. Carbon dioxide reforming of methane over nickel/alkaline earth metal oxide catalysts. Appl Catal A 1995;133:149–61.
[22] Chen YG, Tomishige K, Yokoyama K, Fujimoto K. Catalytic performance and catalyst structure of nickel-magnesia catalysts for $CO_2$ reforming of methane. J Catal 1999;184:479–90.
[23] Feng J, Ding Y, Guo Y, Li X, Li W. Calcination temperature effect on the adsorption and hydrogenated dissociation of $CO_2$ over the NiO/MgO catalyst. Fuel 2012;109:110–5.
[24] Balakrishnan N, Joseph B, Bhethanabotla VR. Effect of Pt and Ru promoters on deactivation of Co catalysts by C deposition during Fischer–Tropsch synthesis: a DFT study. Appl Catal A 2013;462–463:107–15.
[25] Liu H, Zhang R, Ding F, Yan R, Wang B, Xie K. A first-principles study of C + O reaction on NiCo(111) surface. Appl Surf Sci 2011;257:9455–60.
[26] Zhang R, Liu H, Wang B, Ling L. Insight into the effect of surface hydroxyls on $CO_2$ hydrogenation over Pd/γ-$Al_2O_3$ catalyst: a computational study. Appl Catal B 2012;126:108–20.
[27] Nørskov JK, Bligaard T, Rossmeisl J, Christensen CH. Towards the computational design of solid catalysts. Nat Chem 2009;1:37–46.
[28] Wang SG, Liao XY, Hu J, Cao DB, Li YW, Wang J, et al. Kinetic aspect of $CO_2$ reforming of $CH_4$ on Ni(111): a density functional theory calculation. Surf Sci 2007;601:1271–84.
[29] Burghgraef H, Jansen APJ, van Santen RA. Electronic structure calculations and dynamics of the chemisorption of methane on a Ni(111) surface. Chem Phys 1993;177:407–20.
[30] Abild-Pedersen F, Lytken O, Engbæk J, Nielsen G, Chorkendorff I, Nørskov JK. Methane activation on Ni(111): Effects of poisons and step defects. Surf Sci 2005;590:127–37.
[31] Moussounda PS, Haroun MF, M'passi-Mabiala B, Légaré P. A DFT investigation of methane molecular adsorption on Pt(100). Surf Sci 2005;594:231–9.
[32] Bunnik BS, Kramer GJ. Energetics of methane dissociative adsorption on Rh(111) from DFT calculations. J Catal 2006;242:309–18.
[33] Valero MC, Raybaud P, Sautet P. Interplay between molecular adsorption and metal-support interaction for small supported metal clusters: CO and $C_2H_4$ adsorption on $Pd_4$/γ-$Al_2O_3$. J Catal 2007;247:339–55.
[34] Yang J, Lv CQ, Guo Y, Wang GC. A DFT+U study of acetylene selective hydrogenation on oxygen defective anatase (101) and rutile (110) $TiO_2$ supported $Pd_4$ cluster. J Chem Phys 2012;136:104107/1–104107/15.
[35] Teng BT, Wu FM, Huang WX, Wen XD, Zhao LH, Luo MF. A DFT study of the structures of $Au_x$ clusters on a $CeO_2$(111) surface. ChemPhysChem 2012;13:1261–71.
[36] Teng BT, Lang JJ, Wen XD, Zhang C, Fan M, Harris HG. $O_2$ adsorption and oxidative activity on gold-based catalysts with and without a Ceria support. J Phys Chem C 2013;117(18986–18993):18993.
[37] López N, Illas F. Ab initio modeling of the metal-support interface: the interaction of Ni, Pd, and Pt on MgO(100). J Phys Chem B 1998;102:1430–6.
[38] Wang Y, Truong TN. Cluster formation model in vapor deposition of Pd atoms on the perfect MgO(100) surface and on its surface oxygen vacancy. J Phys Chem C 2008;112:13674–80.
[39] Payne MC, Allan DC, Arias TA, Joannopoulos JD. Iterative minimization techniques for ab initio total-energy calculations: molecular dynamics and conjugate gradients. Rev Mod Phys 1992;64:1045–97.
[40] Milman V, Winkler B, White JA, Pickard CJ, Payne MC, Akhmatsakaya EV, et al. Electronic structure properties and phase stability of inorganic crystals: a pseudopotential plane-wave study. Int J Quantum Chem 2000;77:895–910.
[41] Perdew JP, Burke K, Ernzerhof M. Generalized gradient approximation made simple. Phys Rev Lett 1996;77:3865–8.
[42] Vanderbilt D. Soft self-consistent pseudopotentials in a generalized eigenvalue formalism. Phys Rev B 1990;41:7892–5.
[43] Monkhorst HJ, Pack JD. Special points for brillouin-zone integrations. Phys Rev B 1976;13:5188–92.
[44] Halgren TA, Lipscomb WN. The synchronous-transit method for determining reaction pathways and locating molecular transition states. Chem Phys Lett 1977;49:225–32.
[45] Pan Y, Liu C, Ge Q. Effect of surface hydroxyls on selective $CO_2$ hydrogenation over $Ni_4$/γ–$Al_2O_3$: A density functional theory study. J Catal 2010;272:227–34.
[46] Carneiro JWM, Cruz MTM. Density functional theory study of the adsorption of formaldehyde on $Pd_4$ and on $Pd_4$/γ–$Al_2O_3$ clusters. J Phys Chem A 2008;112:8929–37.
[47] Zhang R, Wang B, Liu H, Ling L. Effect of surface hydroxyls on $CO_2$ hydrogenation over Cu/γ–$Al_2O_3$ catalyst: A theoretical study. J Phys Chem C 2011;115:19811–8.
[48] Alfonso DR, Snyder JA, Jaffe JE, Hess AC, Gutowski M. Opposite rumpling of the MgO and CaO(100) surfaces: a density-functional theory study. Phys Rev B 2000;62:8318–22.
[49] Wang B, Yan R, Liu H. Effects of interactions between NiM (M = Mn, Fe, Co and Cu) bimetals with MgO(100) on the adsorption of $CO_2$. Appl Surf Sci 2012;258:8831–6.
[50] Wang Y, Florez E, Mondragon F, Trong TN. Effects of metal-support interactions on the electronic structures of metal atoms adsorbed on the perfect and defective MgO(100) surface. Surf Sci 2006;600:1703–13.
[51] Ferrari AM, Giordano L, Pacchioni G, Abbet S, Heiz U. Selectivity of surface defects for the activation of supported metal atoms: acetylene cyclotrimerization on $Pd_1$/MgO. J Phys Chem B 2002;106:3173–81.
[52] Li J, Croiset E, Ricardez-Sandoval L. Effect of metal-support interface during $CH_4$ and $H_2$ dissociation on Ni/γ–$Al_2O_3$: A density functional theory study. J Phys Chem C 2013;117:16907–20.
[53] Hammer B, Nørskov JK. Electronic factors determining the reactivity of metal surface. Surf Sci 1995;343:211–20.
[54] Mavrikakis M, Hammer B, Nørskov JK. Effect of strain on the reactivity of metal surface. Phys Rev Lett 1998;81:2819–22.
[55] Skoplyak O, Barteau MA, Chen JG. Reforming of oxygenates for $H_2$ production: Correlating reactivity of ethylene glycol and ethanol on Pt(111) and Ni/Pt(111) with surface *d*-band center. J Phys Chem B 2006;110:1686–94.
[56] Bradford MCJ, Vannice MA. Catalytic reforming of methane with carbon dioxide over Nickel catalysts I. Catalyst characterization and activity. Appl Catal A 1996;142:73–96.
[57] Tomishige K, Yamazaki O, Chen Y, Yokoyama K, Li X, Fujimoto K. Development of ultra-stable Ni catalysts for $CO_2$ reforming of methane. Catal Today 1998;45:35–9.
[58] Wang YH, Liu HM, Xu BQ. Durable Ni/MgO catalysts for $CO_2$ reforming of methane: activity and metal-support interaction. J Mol Catal A 2009;299:44–52.
[59] Osaki T, Masuda H, Mori T. Intermediate hydrocarbon species for the $CO_2$–$CH_4$ reaction on supported Ni catalysts. Catal Lett 1994;29:33–7.
[60] Bradford MCJ, Vannice MA. Catalytic reforming of methane with carbon dioxide over nickel catalysts II. Reaction kinetics. Appl Catal A 1996;142:97–122.
[61] Wei J, Iglesia E. Isotopic and kinetic assessment of the mechanism of reactions of $CH_4$ with $CO_2$ or $H_2O$ to form synthesis gas and carbon on nickel catalysts. J Catal 2004;224:370–83.
[62] Wang S-G, Liao X-Y, Jia H, Cao D-B, Li Y-W, Wang J, et al. Kinetic aspect of $CO_2$ reforming of $CH_4$ on Ni(111): a density functional theory calculation. Surf Sci 2007;601:1271–84.
[63] Rostrup-Nielsen JR, Hansen JHB. $CO_2$-reforming of methane over transition metals. J Catal 1993;144:38–49.
[64] Chen JX, Qiu YJ, Zhang JY, Su WH. Influence of $La_2O_3$ and $CeO_2$ promoters on physico-chemical properties and catalytic performance of Ni/MgO catalyst in methane reforming with carbon dioxide. Acta Phys Chim Sin 2004;20:76–80.